Recent Strategies for Improving the Catalytic Activity of 2D TMD Nanosheets Toward the Hydrogen Evolution Reaction

*Damien Voiry, Jieun Yang, and Manish Chhowalla**

Two-dimensional (2D) transition-metal dichalcogenide (TMD) nanosheets have emerged as a fascinating new class of materials for catalysis. These nanosheets are active for several important catalysis reactions including hydrogen evolution from water. The rich chemistry of TMDs combined with numerous strategies that allow tuning of their electronic properties make these materials very attractive for understanding the fundamental principles of electro- and photocatalysis, as well as for developing highly efficient, renewable, and affordable catalysts for large-scale production of hydrogen. Recent developments are highlighted and important challenges in using TMDs as catalysts are also discussed.

1. Introduction

In the past 10 years, two dimensional (2D) materials have become the focus of researchers working on nanomaterials because of their interesting optical and electronic properties that arise from the absence of the third dimension. The interesting surface and electronic properties of 2D materials have been widely studied and applied to a variety of proof-of-concept devices. One avenue of research that seems particularly promising with 2D transition-metal dichalcogenides (TMDs) is electrocatalysis for the hydrogen evolution reaction (HER). A key advantage of 2D TMDs is that all of the catalytically active sites are exposed due to the atomically thin nature of the nanosheets. Layered TMDs consist of alternating sheets of transition-metal atoms sandwiched between two chalcogen atoms. The oxidation degree of the metal and the chalcogen atoms is +4 and −2, respectively. The difference in oxidation degree induces the formation of strong ionic bonds between the metal and the chalcogen atoms, which preserve the structure of the nanosheets, whereas the existence of weak van der Waals bonds between the individual layers enables the exfoliation of bulk crystals down to single layers. A variety of compounds with different transition metals and chalcogens can be realized.[1] The variations in chemistry of the compounds leads to dramatic differences in their catalytic activity, providing a rich platform for studying the fundamental properties, as well as laying the ground work for future technologies. In addition to the compositional tunability, the crystal structure and strain can also be varied to enhance the catalytic performance of 2D-TMD-based catalysts for the HER.[2–5] Such strategies have already been applied in electronic and optical devices for improving the performance and studying fundamental behavior of the materials,[6–10] but fewer examples have been reported for electrocatalysis. In this article, we present recent developments in TMDs for electro- and photocatalysis for the production of hydrogen.

2. TMDs as Electrocatalysts for the HER

2.1. Hydro-desulfurization Reaction using TMDs

Early studies have shown that TMDs and in particular MoS_2 are useful catalysts in hydro-desulfurization (HDS) reactions.[11] Initial studies of the HDS reaction using scanning tunneling microscopy (STM) and thiophene as the reactant have revealed that adsorption occurs at the edges of the TMDs.[12] TMDs possess edges that comprise chalcogen or transition-metal atoms.[13] Edges can also be covered with 0%, 50%, 75%, or 100% of chalcogen atoms, depending on the synthesis conditions and the size of the nanosheets.[14,15] STM images of MoS_2 nanoclusters reveal bright brims, indicating that the 1D edges are metallic, as confirmed by DFT calculations.[16] Understanding the edge structure and conductivity has been important in elucidating the fundamental HDS reaction mechanisms.[17,18]

2.2. MoS_2 as a Hydrogen-Evolution Catalyst

In electro- and heterocatalysis, the reactivity is correlated to the adsorption energy (**Figure 1**a). According to the Sabatier principle, the interactions between catalysts and reactants should neither be too strong nor too weak, for the reaction to proceed efficiently.[19] If the free energy of adsorption is too high then the binding is not efficient and the reaction is rate-limited by the adsorption of the reactant. On the other hand if ΔG_{H^*} is too strong, then the conversion and desorption are slow, leading to poisoning of the catalyst surface. In 2005, Hinnemann et al. used DFT calculations to estimate the free energy of hydrogen adsorption (ΔG_{H^*} on the MoS_2 edge[20]), which revealed that ΔG_{H^*} is indeed close to thermo-neutral, making MoS_2 potentially promising as an HER catalyst.[20] The theory results were

---

Dr. D. Voiry, Dr. J. Yang, Prof. M. Chhowalla
Department of Materials Science and Engineering
Rutgers
The State University of New Jersey
NJ, USA
E-mail: manish1@rci.rutgers.edu

DOI: 10.1002/adma.201505597

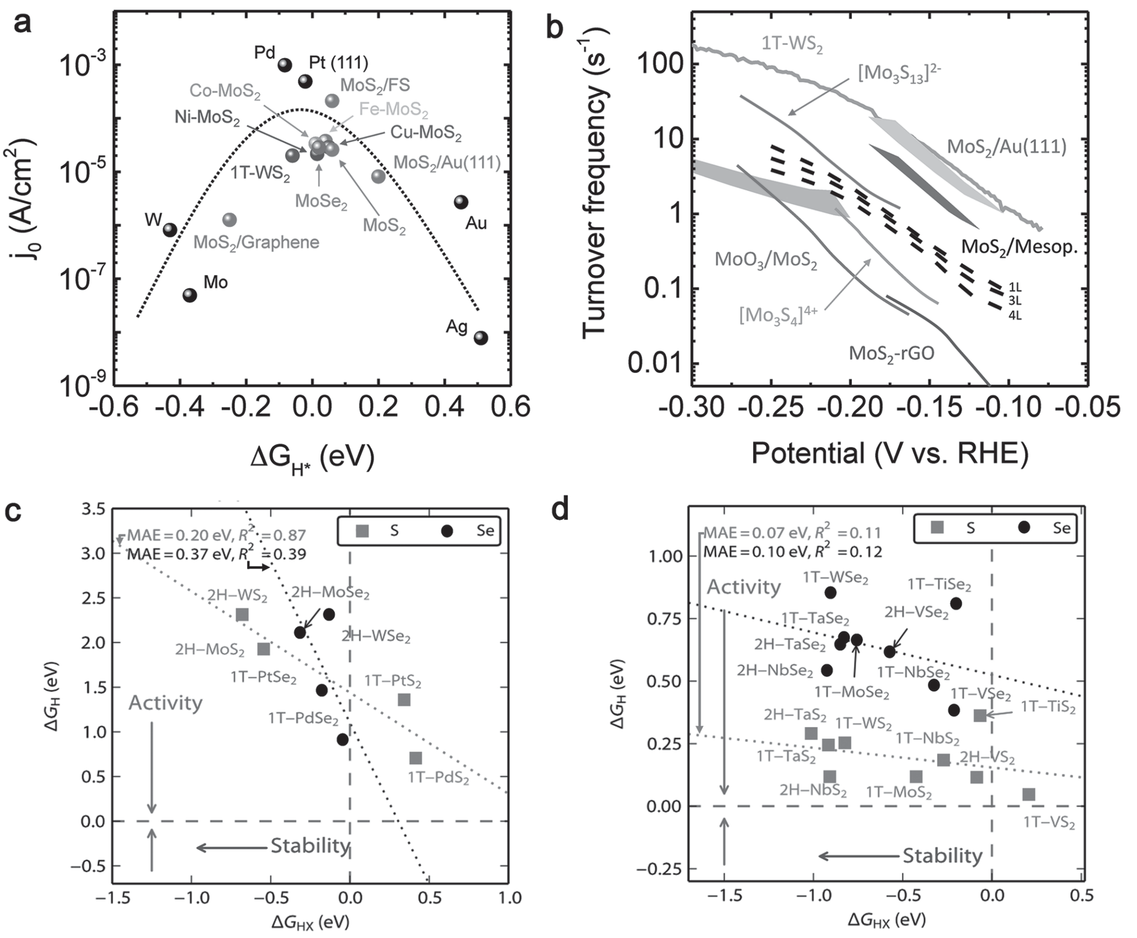

Figure 1. Thermodynamics of hydrogen adsorption on 2D transition metal dichalcogenides. a) Sabatier "volcano" plot showing the exchange current density as a function of free energy of hydrogen adsorption of free-standing (FS) MoS_2 edges, MoS_2 edges on Au (111), MoS_2 edges on graphene, vertically grown Fe, Cu, Ni, Co-promoted MoS_2 edges, vertically grown MoS_2 edges[32], vertically grown $MoSe_2$ edges,[27] 1T WS_2 basal plane,[2] and compared with various metals. Data taken from refs.[2,27,32,33] b) Evolution of turnover frequency of several catalysts based on transition-metal chalcogenides with overpotential. Data taken from refs.[2,23,24,26,34,35,29] c,d) Plots of ΔG_{H^*}: the free energy of hydrogen adsorption as function of ΔG_{HX} (X = S or Se): the HX adsorption free energy. c,d) The evolution is displayed for metallic TMDs (c) and semiconducting TMDs (d). In general the stronger binding of X ($\Delta G_{HX} < 0$), the higher stability of TMDs, the lower the reactivity of TMDs ($\Delta G_{H^*} > 0$), the weaker the hydrogen binding. c,d) Reproduced with permission.[36] Copyright 2015, Elsevier.

confirmed experimentally by electrochemical measurements on MoS_2 particles grown on graphite.[20] Bonde et al. calculated the free energy of hydrogen adsorption on the Mo and S edges of the MoS_2.[21] These values have been further refined recently by Nørskov's group.[22] The results show that the best edge configurations correspond to Mo edges covered by 50% S with $\Delta G_{H^*} = 0.06$ eV compared to S edges covered by 100% S: $\Delta G_{H^*} = -0.45$ eV.[22] WS_2 edges have also been found to be active with $\Delta G_{H^*} = -0.04$ and -0.06 eV for 50% W edges and 100% S edges, respectively.[22] Experimental evidence on the crucial role of edges in the HER was obtained by Jaramillo et al. who correlated the electrochemical activity and edge length of MoS_2 nanoclusters measured by STM.[23] They also obtained the exchange current density per active site and the turnover frequency (TOF) (the number of hydrogen molecules/atoms per second. being produced per active site per second) using the same measurements. The TOF at equilibrium potential reaches ca. 0.02 s^{-1} for the MoS_2 edges compared with 0.9 s^{-1} for Pt (111) and rapidly increases with the overpotential (Figure 1b, grey regions). These pioneering experiments provided evidence that MoS_2 catalysts perform just below noble metals such as Pd or Pt in the Sabatier volcano plot (Figure 1a) as catalysts for the HER.[23] These initial results have led to substantial effort being devoted by the scientific community to increase the concentration of conducting edges to enhance their catalytic performance.[24–29] Evidence for edge activity has been provided using various experiments, including recent work showing preferential electro-deposition of Li_2S on edges due to strong binding relative to the surface of the nanosheets.[30] Higher and faster electrochemical response of edge sites compared to the basal planes are also obtained upon exposure to $[Fe(CN)_6]^{3+/4+}$ or $[Ru(NH_3)_6]^{3+/2+}$ redox couples and attributed to higher activity from the edge sites.[31]

2.3. Other Catalytically Active TMDs

Sulfur- and selenium-based TMDs from group VI are expected to follow the same trends as MoS_2 because of minimal changes

DOI: 10.1002/adma.201505597

in the thermodynamics of hydrogen binding between the different transition metals and chalcogens.[22] In electrocatalysis, the catalytic activity and stability of the active sites are important. The stability of the edges or the basal planes can be predicted from calculations of H–X (where X = S or Se is the adsorption-site atom) adsorption free energy, $\Delta G_{\text{H–X}}$. For $\Delta G_{\text{H–X}} > 0$, desorption of H–X groups in the form of H_2X becomes favorable. $\Delta G_{\text{H–X}}$ is generally inversely proportional to the energy of hydrogen adsorption. In other words, a less stable catalyst ($\Delta G_{\text{H–X}} > 0$) possesses strong hydrogen binding ($\Delta G_{\text{H*}} < 0$). Tsai et al. recently calculated the free energy of hydrogen adsorption, as well as the free energy of H–X adsorption to estimate the catalytic activity and the stability of the edges and basal planes of various 2D TMDs (Figure 1c,d).[36] The evolution of the stability with activity on the basal plane is significantly lower in the case of metallic TMDs compared with that of semiconducting TMDs. This suggests that TMDs with active ($\Delta G_{\text{H*}} \approx 0$) basal planes are also electrochemically more stable.[36] Very interestingly, these results indicate that the basal planes of TMDs can be catalytically activated for metallic TMDs with free energy of hydrogen adsorption as low as 0.05 eV in the case of 1T phase VS_2 (Figure 1d). These calculations open new avenues for improving the HER activity of 2D TMDs.

3. Strategies for Improving the HER Activity of TMDs

3.1. Edge Engineering of MoS_2 and Other TMDs

The observation of MoS_2 edge activity for the HER has opened new avenues for increasing catalyst performance by optimizing the basal plane to edge ratio. Several routes for improving the density of accessible edges at the surface of TMDs have been proposed in the past few years. They typically involve engineering the surface of the catalysts to expose edges, or introducing structural defects to create new surfaces with edges (e.g., creating holes).[37–40] One such strategy to this end is the synthesis of high-surface-area MoO_3 nanowires that are converted to MoS_2 by sulfidation.[25] This method creates high-surface electrodes with a substantial fraction of edge-exposed MoS_2, which shows effective performance toward the HER. Kibsgaard et al. have reported an elegant method to prepare mesoporous MoS_2 from MoO_3 using a double-gyroid silica template.[26] Characterization of the mesoscopic structure reveals that the surface is predominantly composed of MoS_2 edges. Despite this, the decrease in the HER activity with increasing number of layers suggests that optimization of the edge concentration is still not ideal in these structures (Figure 1b, light blue curve). The decrease in catalytic activity with the number of layers was investigated by Yu et al., who reported that the activity of MoS_2 catalysts decreases by 4.5 times when adding a layer of MoS_2 due to the large potential required for electron hopping between successive layers (**Figure 2**a,b).[41] A similar trend was observed by Seo et al., although the authors of the study attribute the better performance to the modification of the electronic structure of MoS_2 nanosheets with decreasing number of layers (Figure 1b, dashed curves).[34] Recent progress on chemical vapor deposition (CVD) of TMDs allows careful examination of the catalytic process on single-layer materials with well-defined edge and basal plane structures. MoS_2 nanosheets can be grown on or transferred onto conducting substrates and studied for the HER. However, due to the large size of the crystals, the edge to basal sites ratio is significantly lower than in the case of nanoclusters.[23] Zhang et al. reported the growth of MoS_2 having a fractal morphology (Figure 2c,d).[42] The performance of MoS_2 electrodes increases with the dendritic character of the edges (Figure 2e). Alternatively, nanosheets can be grown vertically since the in-plane conductivity of the basal plane is >2000 times higher than of the out-of-plane configuration between the layers. This approach constitutes a promising method to synthesize MoX_2 (X = S or Se), which combines a high density of edges and an improved electron mobility of the electrode materials.[43] Cui's group at Stanford demonstrated the growth of vertically aligned TMDs nanosheets by CVD on various substrates.[27,44] From the HER results and the structural characterization based on transmission electron microscopy, TOFs at 0 V reach 0.013 and 0.014 s^{-1} for vertically aligned MoS_2 and $MoSe_2$ films, respectively, in good agreement with Jaramillo's values (Figure 1a).[27]

3.2. Defect Engineering in TMDs Nanosheets

The high catalytic activity of the edges is thought to originate from unsaturated sulfur atoms at the edges. This has led to the synthesis of amorphous TMDs that presumably have a high concentration of unsaturated sulfur atoms.[45,46] Alternatively, edge sites can be created by increasing the density of structural defects on the nanosheets (Figure 2f,g).[37,47] Numerous types of defects have been observed in single-layer TMDs[15,48] and studied using STEM. Defects are known to dramatically perturb the local density of states and create additional energy levels between the valence and conduction bands.[15,48] So far, very limited number of investigations have focused on the importance of defects on the HER activity of TMDs. The understanding of the role of defects and their controlled synthesis can potentially open new directions for increasing the density of active sites or increasing the conductivity of basal planes of the nanosheets.

4. Emerging Strategies for Enhancing the HER Activity

4.1. Phase Engineering in TMDs

It is known that the electronic structure strongly influences the catalytic properties of materials.[49] TMDs offer opportunities for varying and therefore testing different atomic and electronic structures. For example, MoS_2 or WS_2 nanosheets can be prepared with semiconducting trigonal prismatic (2H phase) or metallic octahedral (1T phase) structures by increasing the electron density in the d orbitals of the metal atoms (**Figure 3**a).[50] Chhowalla's group has investigated the HER activity from chemically exfoliated WS_2 prepared via lithium intercalation.[2] The characterization of the exfoliated materials showed that the nanosheets are predominantly composed of the distorted

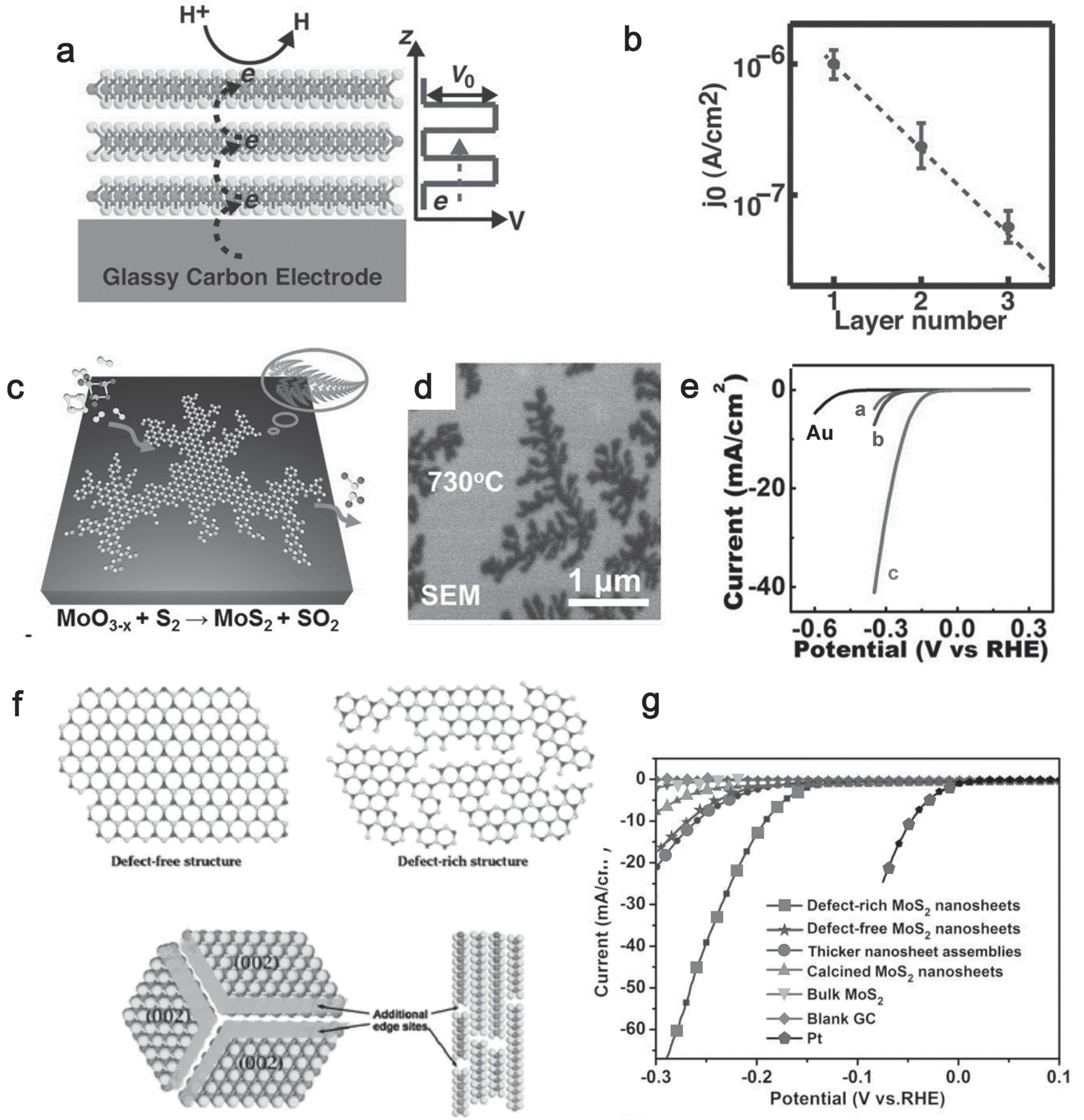

Figure 2. Influence of the number of layers and density of edges on HER activity of MoS_2 electrodes. a) Schematic illustrating the electron hopping between the layers of MoS_2. Extra potential is required for electrons to hop from one layer to one other. Yu et al.[41] estimated the extra-potential, V_0, to be ca. 120 mV. b) Evolution of the exchange current density of MoS_2 with increasing number of layers. a,b) Reproduced with permission.[41] Copyright 2014, American Chemical Society. c,d) Chemical vapor deposition of MoS_2 with fractal edges. e) Polarization curves from various MoS_2 electrodes with 60% (a), 40% (b) and 12% (c) coverages. The improvement in performance is attributed to the higher dendritic character of the MoS_2 nanosheets rather than coverage. c–e) Reproduced with permission.[42] Copyright 2014, American Chemical Society. f) Schematic representation of defect-free and defect-rich MoS_2 nanosheets. g) Polarization curves obtained from MoS_2 nanosheets with various densities of defects. Higher current densities are obtained from defect-rich nanosheets. f,g) Reproduced with permission.[37] Copyright 2013, Wiley-VCH.

metallic 1T phase (1T' phase) with tungsten zig-zag chains characteristic of the ($2a \times a$) superstructure (Figure 3b).[2] They correlated the catalytic performance to the concentration of the 1T phase and the overall strain in the nanosheets. Interestingly, they found that the activity of the electrode is progressively reduced when restoring the 2H phase at the expense of the 1T phase (Figure 3c). DFT calculations revealed that ΔG_{H^*} on the basal plane of 1T-WS_2 is sensitive to the strain. The strain in

DOI: 10.1002/adma.201505597

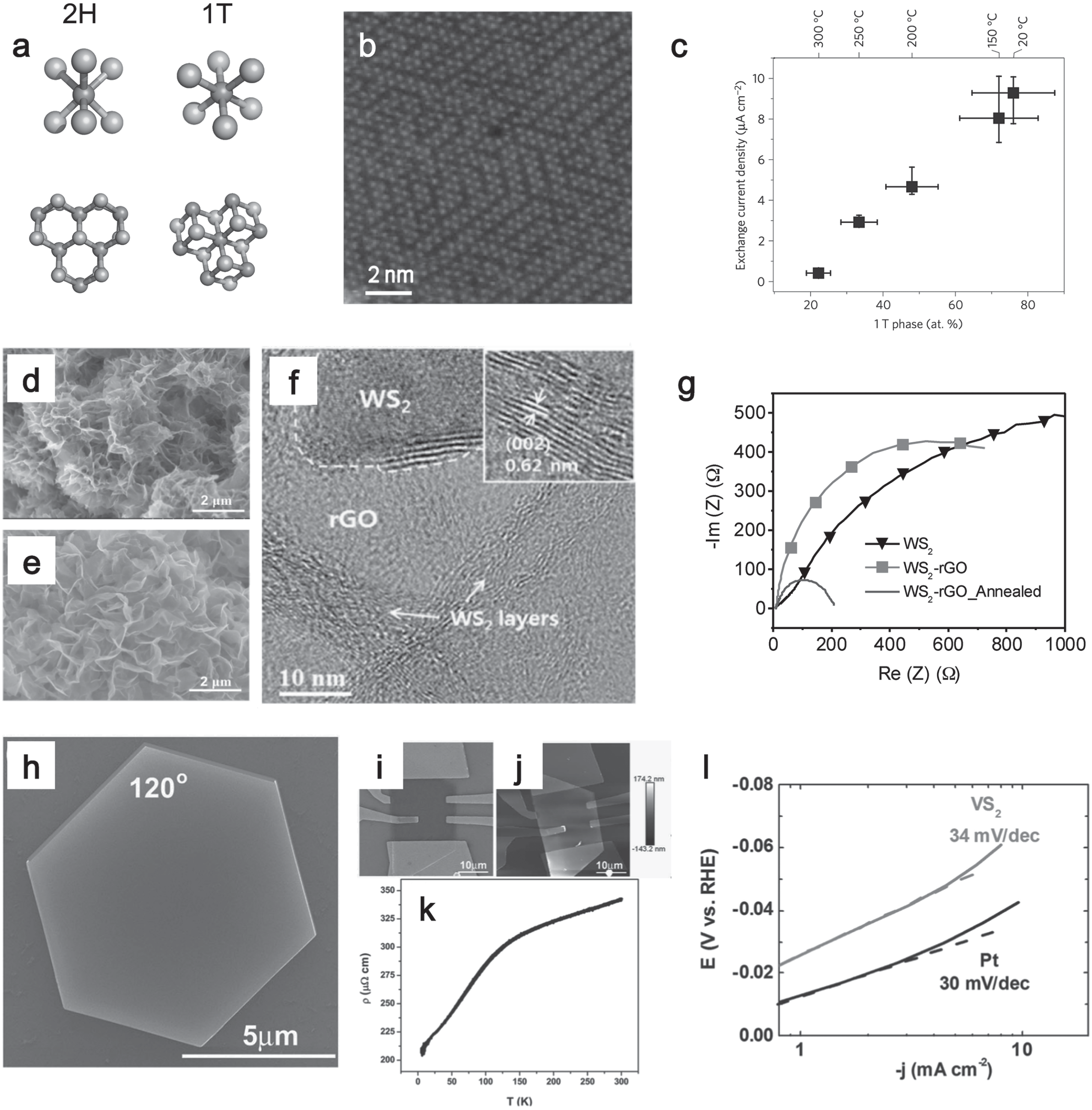

Figure 3. Phase engineering and importance of the electrical coupling. a) Crystal structures from the 2H and 1T phases that correspond to trigonal prismatic and octahedral coordination of the transition metal, respectively. b) Scanning transmission electron microscopy (STEM) image of chemically exfoliated strained 1T-WS_2 exhibiting typical ($2a \times a$) superlattice. c) Evolution of exchange current density of WS_2 nanosheets with increasing concentration of 1T phase. a–c) Reproduced with permission.[2] Copyright 2013, Nature Publishing Group. d,e) Scanning electron microscopy (SEM) images for WS_2 (d), WS_2–rGO hybrids (e). f) High-resolution transmission electron microscopy (HRTEM) images of WS_2–rGO hybrids showing both in-plane and out-of-plane configurations for the WS_2 nanosheets on rGO. g) Nyquist plot of the WS_2, WS_2–rGO and annealed WS_2–rGO electrodes demonstrating the decrease of the charge-transfer resistance when improving the electrical coupling between the rGO and the WS_2. d–f) Reproduced with permission.[51] Copyright 2013, Wiley-VCH. h–j) SEM images of CVD-grown VS_2 nanosheets and VS_2-based electronic devices. k) Evolution of the conductivity of VS_2 with temperature. l) Tafel plots obtained from VS_2. Tafel slopes as low as 34 mV dec^{-1} have been obtained thanks to the metallic character of VS_2. g–l) Reproduced with permission.[52] Copyright 2015, Wiley-VCH.

turn is related to the increase in the density of states below the Fermi level. For a tensile strain of ca. 2.7% the hydrogen adsorption was calculated to be thermo-neutral. Similar enhancement of the HER activity has been observed for exfoliated MoS_2 when converting the 2H phase to the 1T phase.[3–5] The results also agree with recent calculations from Nørskov's group on the energy of hydrogen adsorption on the basal planes of metallic TMDs.[36]

The ideal TiS_2-type 1T phase of MoS_2 is theoretically predicted to be unstable and should relax to the distorted ($2a \times a$, also noted $\sqrt{3}a \times a$) superstructure. However, Eda et al.[53] and others[54] have experimentally observed 1T and distorted 1T phases in chemically exfoliated nanosheets. The 1T phase is metallic, whereas the ($2a \times a$) distorted 1T phase is a narrow-energy-gap semiconductor with a bandgap of few tens of meV.[54–56] Clear identification of the 1T phase and distorted 1T (1T') phase is often missing in the literature. Raman spectroscopy can be used to identify the distorted 1T phase using the additional vibration modes that originate from the zig-zag clustering of the metal atoms due to distortions.[57,58] Observations of these Raman signatures have been reported in several different studies, suggesting that the 1T' phase of MoS_2 is indeed distorted.[3–5]

4.2. Effect of Doping and Strain on HER Activity

The electronic properties of TMDs are largely tunable by chemical modifications, such as strain engineering or doping.[59–63] In the bulk, most dopants are trapped within the structure and are not available on the surface, which is where the catalytic reactions occur. However, in the case of nanosheets, dopants are present on or very close to the surface of the materials and play an active role in the catalysis reaction. For instance, the catalytic properties of graphene can be dramatically enhanced by inserting nitrogen, boron, sulfur, and phosphorus into the carbon lattice.[64] Doping can be used to tune the energy of hydrogen adsorption. Early experiments carried out on MoS_2 nanoclusters used transition metals such as Co or Ni as dopants.[18,21] The morphology of the particles is largely perturbed by the incorporation of cobalt atoms, and STM analyses have shown that the Co–MoS_2 nanoclusters are more truncated.[18] Recently the energy of hydrogen adsorption has been calculated for the Mo and S edges of MoS_2 promoted with nickel, copper, cobalt, and iron.[32] The results show that the energy to adsorb hydrogen on promoted MoS_2 is dramatically affected by the presence of heteroatoms. The ideal scenario corresponds to cobalt-doped MoS_2 catalysts with minimum $\Delta G_{H*} = 0.01$ eV on S-edges (Figure 1a). The substitution of atoms strains the structure of the TMD nanosheets, which profoundly modifies the electronic properties.[65] Kuo's group has studied the influence of biaxial tensile strain of the distorted 1T phase group-VI TMDs on the free energy of hydrogen adsorption.[66] The application of strain increases the density of states near the Fermi level, decreases the energy of hydrogen adsorption, and stabilizes the adsorbed hydrogen at the surface of the basal plane.

4.3. Influence of Catalyst Support Material

The choice of substrates can influence the energy of hydrogen adsorption.[33,67] In general, the stronger the binding between the MoS_2 and the substrate, the weaker the hydrogen adsorption.[67] Tsai et al. calculated the free energy of hydrogen adsorption for MoS_2 supported on various substrates, such as gold, graphene, and MoS_2.[67] Interestingly ΔG_{H*} for the Mo edge on graphene or gold is significantly higher compared to the free-standing Mo-edge: 0.20 eV on Au(111) and 0.24 eV on graphene compared to 0.06 eV for free-standing MoS_2.[67] The estimated theoretical exchange current density (j_0) of unsupported MoS_2 reaches ca. 2×10^{-4} A cm^{-2}, giving a TOF of ca. 0.6 s^{-1}, very close to the TOF of Pt: 0.9 s^{-1} (Figure 1a).[67] This value is also significantly higher than the experimental values obtained from MoS_2 nanoclusters grown on Au (111) (8×10^{-6} A cm^{-2}),[23] suggesting that further improvements in designing appropriate substrates are required to decrease ΔG_{H*} to a thermo-neutral value.

Together with the free energy of hydrogen adsorption, the electrical conductivity of the catalyst is an important parameter in catalytic performance. The energy of hydrogen adsorption is calculated in vacuum conditions for idealized systems. Although ΔG_{H*} provides useful insights into the HER properties; it provides only a partial picture of the HER process at the surface of the nanosheets. Moreover, the exchange current density does not take into account the effectiveness of the substrate (the cathode that provides electrons) and the catalyst to provide an electron to the active site, since, at 0 V, the flow of electrons is greater than the TOF.[68] At higher overpotentials, the TOF increases and the electrical conductivity largely governs the HER activity of the electrode. For this reason, a direct comparison of the catalytic performance of the basal and edges sites of nanosheets remains challenging due to the large difference in electrical properties between the metallic edges and the semiconducting basal plane.[30,31] In poorly conducting materials, an additional potential is required to drive electrons more efficiently to the active sites. This is a major drawback for group-VI TMDs, which typically consist of a semiconducting trigonal prismatic structure. Additionally, because MoS_2 is semiconducting, large Schottky barriers are typically formed between the catalysts and the metallic substrates.[6] Thus, metallic TMDs that form good electrical contact with metallic substrates have natural advantages over semiconducting catalysts. 1T-MoS_2 or WS_2 thin films exhibit a conductivity of ca. 50–100 S cm^{-1} compared with 10^{-5} S cm^{-1} for their 2H phase counterparts.[3,69] Chhowalla's and Jin's groups have shown a large improvement in the catalytic response from the 1T phase.[3,4] The importance of conductivity on the catalytic activity of the 1T phase materials was illustrated in these works by decreasing the Tafel slopes and the lower internal resistances in the Nyquist plots obtained by impedance spectroscopy. The intrinsic conductivity of 2H MoS_2 can be enhanced via doping without inducing phase transformation.[47,70] Alternatively, the catalytic activity of semiconducting TMDs can also be increased by growing the nanosheets on a conducting surface. Li et al. reported the synthesis of MoS_2–rGO (reduced graphene oxide) hybrids via hydrothermal reaction (Figure 1b, blue curve).[35] Similarly Yang et al. reported a method to prepare layered WS_2 from a hydrothermal reaction on rGO (Figure 3d–f). The growth of TMDs on graphene enables a strong anchoring of nanosheets on the graphene basal plane, which improves the electrical communication between the two moieties and leads to a dramatic decrease of the charge-transfer resistance (Figure 3g).[51] Group-V TMDs with the electron count d^1 are typically semi-metallic or metallic. Lou's group reported the synthesis of thin crystals of 1T-VS_2 by CVD (Figure 3h).[52] Owing to its high electrical

Adv. Mater. 2016, DOI: 10.1002/adma.201505597

conductivity of ca. 3000 S cm^{-1} (Figure 3i–k), VS_2 demonstrates high electrocatalytic activity toward the synthesis of hydrogen, with a negligible onset potential and Tafel slopes as low as 34 mV dec^{-1} (Figure 3l).[52]

5. TMDs for Photocatalysis

Since the first report of photoelectrical water-splitting using TiO_2 electrodes, water-splitting for hydrogen production using solar energy has become an important field of research for renewable energy.[71,72] Most semiconducting electrodes are limited by a lack of absorption over the entire solar spectrum, and recombination of electron–hole pairs before hydrogen evolution can occur.[73] So far, MoS_2 and WS_2 have been used as active materials coupled to light-harvesting materials, such as graphitic carbon nitride, n- or p-doped silicon, TiO_2, Eosin Y, or CdS.[74–77] Highly active metallic TMDs such as 1T-MoS_2 can serve as co-catalysts to increase the number of active sites on the photocatalyst.[77] Efficient charge separation can be obtained by coupling TMDs and other materials with energy levels that facilitate charge transfer. TMDs with a range of bandgap values can, in principle, also be integrated together to absorb a large portion of the solar spectrum.[78]

In 2008, Zong et al. demonstrated that the activity of CdS can be greatly increased by mixing with MoS_2.[77] MoS_2/CdS showed a higher rate of hydrogen production than Pt/CdS. The authors suggest that structural coupling between MoS_2 and CdS formed due to S^{2-} anions of each material results in a high photocatalytic activity. (**Figure 4**a) Similarly, MoS_2 loaded onto TiO_2 and CdS has been investigated for H_2 evolution, where TiO_2 and CdS act as both light absorbers and catalysts.[73,79,80] Recently, Chen et al. synthesized transition-metal disulfide nanosheets (MS_2) with lateral sizes ranging from 4 to 10 nm on the Cd-rich (0001) surface of wurtzite CdS nanocrystals.[81] This structure has a large number of MS_2 edge sites that are active for the HER. The photocatalytic performance of WS_2–CdS and MoS_2–CdS nanohybrids toward the HER under visible-light irradiation (>420 nm) is about 16 and 12 times that of pure CdS, respectively. TMDs can broaden the light-harvesting window of photocatalysts toward visible light. The integration of TMDs with TiO_2-based photocatalysts is synergistic because TiO_2 undergoes significant absorption at wavelengths shorter than 400 nm, while the absorption of TMDs can be tuned by the number of layers and by the composition to improve absorption of visible and near infra-red (NIR) wavelengths. For example, MoS_2 nanosheets on TiO_2 nanobelts show enhanced absorption in the visible region compared with pure TiO_2 nanobelts.[78] TiO_2 nanobelts in turn exhibit a hydrogen production rate of 1.6 mmol h^{-1} g^{-1} when loaded with 50 wt% of MoS_2. It is also believed that matching of the energy levels between MoS_2 and TiO_2 favors charge transfer and inhibits recombination of photoelectrons and holes.

The use of ternary composites in which one component is capable of light absorption (CdS or TiO_2) for the generation of an electrochemical potential, one that provides catalytic active sites for hydrogen production (MoS_2 and WS_2), and one to increase the conductivity of the catalysts by using reduced graphene oxide (rGO) has been attempted.[73,79,85,82,86] A typical example was reported by Jaroniec's group who investigated

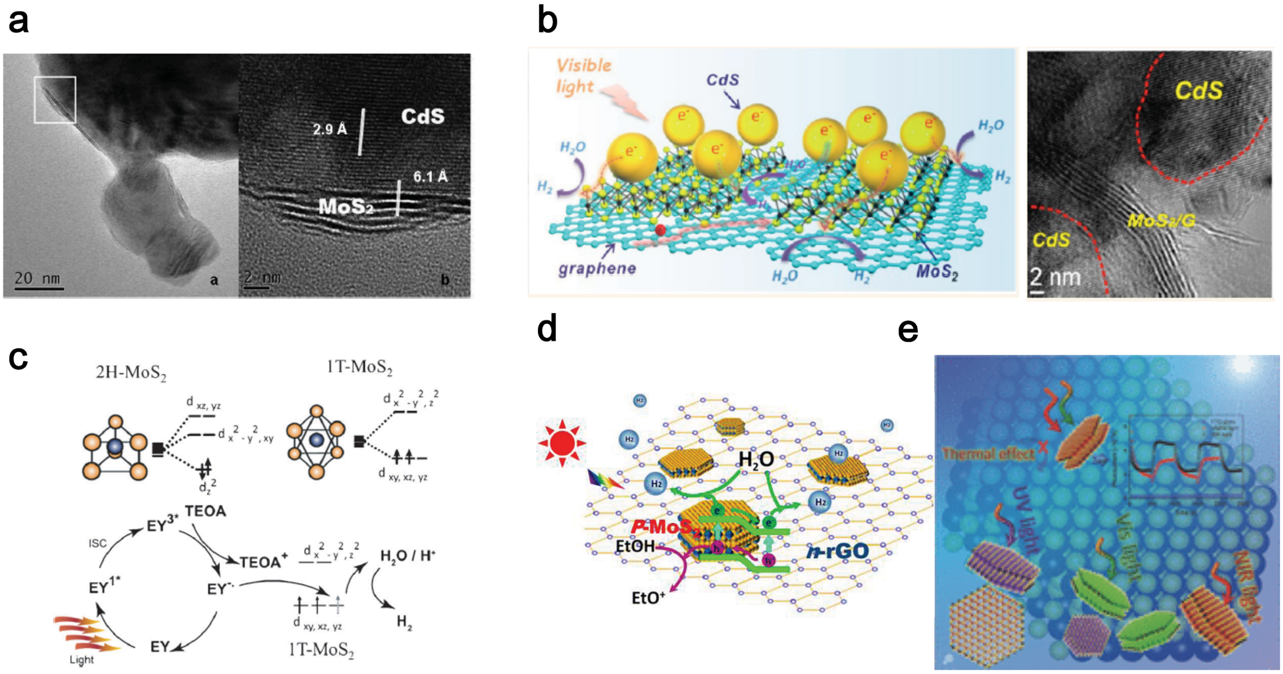

Figure 4. a) HRTEM image of MoS_2/CdS photocatalysts. Reproduced with permission.[77] Copyright 2008, American Chemical Society. b) Schematic illustration and TEM image of MoS_2/rGO/CdS composites. Reproduced with permission.[82] Copyright 2014, American Chemical Society. c) The electronic configuration of 2H-MoS_2 and 1T-MoS_2 and proposed mechanism for photocatalytic activity of 1T-MoS_2.[74] Copyright 2012, Wiley-VCH. d) Scheme for charge generation on p-MoS_2/n-rGO heterostructures. Reproduced with permission.[83] Copyright 2013, American Chemical Society. e) WS_2 nanosheets with strong absorption of UV–vis and NIR light. Reproduced with permission.[84] Copyright 2015, Wiley-VCH.

TiO_2/MoS_2/graphene composites.[73] rGO is useful for facilitating transport of photogenerated electrons from TiO_2 to MoS_2 and to improve the charge-separation properties.[13] Similarly, ternary CdS/MoS_2/graphene hybrid catalysts have shown better photocatalytic activity for water splitting in comparison with single or binary CdS, CdS–MoS_2, and CdS–graphene materials[82,87] (Figure 4b). Maitra et al. reported the first use of 1T-MoS_2 for photocatalysis using eosin as a sensitizer[74] (Figure 4c). 1T-MoS_2 (metallic) displays significantly higher photocatalytic activity than 2H-MoS_2 (semiconducting) and 2H-MoS_2/rGO hybrids reported thus far.[74] Ozin and co-workers demonstrated the direct synthesis of colloidal WS_2 monolayers with 2H and the 1T structure.[88] 1T-WS_2 with TiO_2 as a sensitizer showed a higher rate of H_2 production (2570 µmol g^{-1} h^{-1}) than 2H-WS_2.

A recent study by Bernardi et al. showed that 2D materials can absorb superior amounts of light compared to conventional photovoltaic materials such as silicon or GaAs.[89] Meng et al. also reported high catalytic activity of MoS_2/rGO hybrids in which MoS_2 is the light-harvesting material (Figure 4d).[83] Multi-layer WS_2 with a bandgap of 1.35 eV can expand the light absorption region to 910 nm. To this end, Sang et al. demonstrated that WS_2 nanosheets are active photocatalysts under visible and NIR irradiation for the first time (Figure 4e).[84] Specifically, WS_2 nanoparticles with lateral dimensions of 2–3 µm and thicknesses of ca. 100 nm were prepared by thermal decomposition of $(NH_4)_2WS_4$ at 1200 °C[84] and tested as anodes. **Table 1** summarizes the photocatalytic activities of a variety of MoS_2 and WS_2 catalysts.[73,74,77,79,81,83,85,87,88]

Zhuang et al. calculated the electronic structures of 27 single-layer MX_2 samples[91] Although most single-layer MX_2 structures have band-edge energies that are unfavorable for photocatalytic water splitting without an external bias potential, they suggested that MoS_2, WS_2, PtS_2, and $PtSe_2$ could be promising. Kang et al. demonstrated that the band-edge positions depend on the number of layers of MX_2, and that MoX_2–WX_2 lateral heterostructures have type-II band alignment, making them good candidates for spontaneous photosplitting of water.[92] TMD-based photocatalysts have yet to achieve reasonable activity and stability, and thus the calculations provide important insights toward improving their photocatalytic activity.

6. Stability of TMD Electro- and Photocatalysts

Electrochemical stability is a major concern for electro- or photocatalysts. Group-VI TMDs have demonstrated good stability under HER conditions over 10 000 cycles with minimal increase of the onset potential or the Tafel slope.[25,35] The 1T' phase of group-VI TMDs is known to be less stable than the 2H. Calculations have shown that there is an activation barrier of ca. 1 eV that prevents the fast restoration of the 2H phase.[2,56,93] Experimentally, it has been observed that the transition temperature is relatively high compared to the typical temperatures for the HER: 100 °C and 200 °C for 1T-MoS_2 and 1T-WS_2, respectively.[94] Voiry et al. have shown that 1T phase of WS_2 is stable both in air and in solution over a few months, possibly due to presence of excess charge on the nanosheets and the existence of distortions.[2] Under HER conditions, 1T MoS_2 and 1T WS_2 have been found to be stable over 100 h[2] or 1000 cycles.[4,5] The stability of other TMDs will require further investigation. In the case of group-V TMDs, Yuan et al. have observed good stability over 12 000 cycles, with even a slight improvement of the activity.[52] Nørskov's group has calculated the energy of the H–X adsorption, which predicts the TMD stability during the HER reaction (Figure 1c,d).[36] Most TMDs are found to be stable, but further experimental investigation is required for selecting the most stable TMD catalysts. Similarly, the photostability of TMDs remains largely unexplored. In a recent contribution, Parzinger et al. investigated the stability of MoS_2 under irradiation. Their results suggest that basal planes are stable compared to edges or defect sites. Interestingly edge sites are more stable in multilayer stacks than in single layers.[95]

7. Summary and Outlook

The need for renewable energy has driven efforts for the development of affordable, earth-abundant catalysts for the production

Table 1. TMD cocatalysts for photocatalytic H_2-evolution.

Photocatalyst	Cocatalyst	Synthetic method	Light Source	Reactant solution	Activity [µmol h^{-1} g^{-1}]	Stability	Ref.
CdS	MoS_2	Impregnation sulfidation	≥420 nm (Xe)	Lactic acid	5400	–	[77]
CdSe	MoS_2	Dispersion–adsorption	≥420 nm (Xe)	Na_2S	890	>5 h	[80]
CdS	WS2	Impregnation sulfidation	≥420 nm (Xe)	Lactic acid	4200	<15 h	[90]
TiO_2	MoS_2/rGO	Hydrothermal method	UV–Vis (Xe)	Ethanol	2066	>12 h	[73]
CdS	WS_2 and MoS_2	Wet-chemical mehod	≥420 nm (Xe)	Lactic acid	1984 (WS_2) 1472(MoS_2)	>16 h	[81]
MoS_2	rGO	Hydrothermal method	UV–Vis (Xe)	Ethanol	160	<10 h	[83]
CdS	MoS_2/rGO	Hydrothermal method	≥420 nm (Xe)	Lactic acid	2320	–	[87]
CdS	MoS_2/rGO	Mixing	UV–Vis (Xe)	Lactic acid	3072	–	[85]
CdS	MoS_2/rGO	Hydrothermal and photodeposition	≥420 nm (Xe)	Lactic acid	1236 2231	<4 h	[79]
TiO_2	WS_2	Wet-chemical method	≥420 nm (Xe)	Methanol	2570	>20 h	[88]
Eosin	1T-MoS_2	Chemically exfoliation	UV–Vis (Xe)	TEOA	30 000	<1 month	[74]

DOI: 10.1002/adma.201505597

of hydrogen. TMDs have demonstrated promising properties as electro- and photocatalysts for the HER. TMDs, in particular those from group VI, have been studied for hydro-desulfurization reactions and the HER. In order to improve the catalytic activity of TMD nanosheets, three main strategies are being pursued: i) engineering the structure of 2D TMDs to increase the density of active sites; ii) improving the hydrogen binding on the active sites; and iii) enhancing the electrical coupling and conductivity of the nanosheets to efficiently drive electrons to active sites. Metallic TMDs have natural advantages since they can be active from their basal plane with a free energy for hydrogen adsorption that is close to thermo-neutral, and they offer good electrical conductivity. Besides the enhancement of electrocatalytic properties, TMDs also hold promise as photocatalysts. The rich properties of 2D TMDs can be used to harvest sunlight efficiently, separate electron–hole pairs and drive electrons to active sites to facilitate catalytic reactions. Several key challenges remain for TMD catalysts. Understanding the role of defects, synthesizing TMDs with controlled density of defects and structure,and enhancing their stability are a few examples. The recent progress on the synthesis of single layers and heterostructures of TMDs will allow new possibilities for designing efficient electro- and photocatalysts.

Acknowledgements

D.V. and J.Y. contributed equally to this work. M.C. and D.V. acknowledge financial support from NSF DGE 0903661 and ECCS 1128335. J.Y. and M.C. acknowledge financial support from the Rutgers Energy Institute.

Received: November 12, 2015
Revised: December 8, 2015

---

[1] M. Chhowalla, H. S. Shin, G. Eda, L.-J. Li, K. P. Loh, H. Zhang, *Nat. Chem.* **2013**, *5*, 263.
[2] D. Voiry, H. Yamaguchi, J. Li, R. Silva, D. C. B. Alves, T. Fujita, M. Chen, T. Asefa, V. B. Shenoy, G. Eda, M. Chhowalla, *Nat. Mater.* **2013**, *12*, 850.
[3] D. Voiry, M. Salehi, R. Silva, T. Fujita, M. Chen, T. Asefa, V. B. Shenoy, G. Eda, M. Chhowalla, *Nano Lett.* **2013**, *13*, 6222.
[4] M. A. Lukowski, A. S. Daniel, F. Meng, A. Forticaux, L. Li, S. Jin, *J. Am. Chem. Soc.* **2013**, *135*, 10274.
[5] H. Wang, Z. Lu, S. Xu, D. Kong, J. J. Cha, G. Zheng, P.-C. Hsu, K. Yan, D. Bradshaw, F. B. Prinz, Y. Cui, *Proc. Natl. Acad. Sci. USA* **2013**, *110*, 19701.
[6] R. Kappera, D. Voiry, S. E. Yalcin, B. Branch, G. Gupta, A. D. Mohite, M. Chhowalla, *Nat. Mater.* **2014**, *13*, 1128.
[7] S. Cho, S. Kim, J. H. Kim, J. Zhao, J. Seok, D. H. Keum, J. Baik, D.-H. Choe, K. J. Chang, K. Suenaga, S. W. Kim, Y. H. Lee, H. Yang, *Science* **2015**, *349*, 625.
[8] P. Johari, V. B. Shenoy, *ACS Nano* **2012**, *6*, 5449.
[9] H. J. Conley, B. Wang, J. I. Ziegler, R. F. Haglund, S. T. Pantelides, K. I. Bolotin, *Nano Lett.* **2013**, *13*, 3626.
[10] K. He, C. Poole, K. F. Mak, J. Shan, *Nano Lett.* **2013**, *13*, 2931.
[11] C. Song, *Catal. Today* **2003**, *86*, 211.
[12] M. Salmeron, G. A. Somorjai, A. Wold, R. Chianelli, K. S. Liang, *Chem. Phys. Lett.* **1982**, *90*, 105.
[13] J. V. Lauritsen, J. Kibsgaard, S. Helveg, H. Topsøe, B. S. Clausen, E. Lægsgaard, F. Besenbacher, *Nat. Nanotechnol.* **2007**, *2*, 53.
[14] L. P. Hansen, Q. M. Ramasse, C. Kisielowski, M. Brorson, E. Johnson, H. Topsøe, S. Helveg, *Angew. Chem. Int. Ed.* **2011**, *50*, 10153.
[15] W. Zhou, X. Zou, S. Najmaei, Z. Liu, Y. Shi, J. Kong, J. Lou, P. M. Ajayan, B. I. Yakobson, J.-C. Idrobo, *Nano Lett.* **2013**, *13*, 2615.
[16] M. V. Bollinger, J. V. Lauritsen, K. W. Jacobsen, J. K. Nørskov, S. Helveg, F. Besenbacher, *Phys. Rev. Lett.* **2001**, *87*, 196803.
[17] L. S. Byskov, J. K. Nørskov, B. S. Clausen, H. Topsøe, *J. Catal.* **1999**, *187*, 109.
[18] J. V. Lauritsen, J. Kibsgaard, G. H. Olesen, P. G. Moses, B. Hinnemann, S. Helveg, J. K. Nørskov, B. S. Clausen, H. Topsøe, E. Lægsgaard, F. Besenbacher, *J. Catal.* **2007**, *249*, 220.
[19] P. Sabatier, *La Catalyse En Chimie Organique*, Paris & Liége Ch. Béranger Editeur, Paris, France, **1920**.
[20] B. Hinnemann, P. G. Moses, J. Bonde, K. P. Jørgensen, J. H. Nielsen, S. Horch, I. Chorkendorff, J. K. Nørskov, *J. Am. Chem. Soc.* **2005**, *127*, 5308.
[21] J. Bonde, P. G. Moses, T. F. Jaramillo, J. K. Nørskov, I. Chorkendorff, *Faraday Discuss.* **2008**, *140*, 219.
[22] C. Tsai, K. Chan, F. Abild-Pedersen, J. K. Nørskov, *Phys. Chem. Chem. Phys.* **2014**, *16*, 13156.
[23] T. F. Jaramillo, K. P. Jørgensen, J. Bonde, J. H. Nielsen, S. Horch, I. Chorkendorff, *Science* **2007**, *317*, 100.
[24] T. F. Jaramillo, J. Bonde, J. Zhang, B.-L. Ooi, K. Andersson, J. Ulstrup, I. Chorkendorff, *J. Phys. Chem. C* **2008**, *112*, 17492.
[25] Z. Chen, D. Cummins, B. N. Reinecke, E. Clark, M. K. Sunkara, T. F. Jaramillo, *Nano Lett.* **2011**, *11*, 4168.
[26] J. Kibsgaard, Z. Chen, B. N. Reinecke, T. F. Jaramillo, *Nat. Mater.* **2012**, *11*, 963.
[27] D. Kong, H. Wang, J. J. Cha, M. Pasta, K. J. Koski, J. Yao, Y. Cui, *Nano Lett.* **2013**, *13*, 1341.
[28] D. R. Cummins, U. Martinez, R. Kappera, D. Voiry, A. Martinez-Garcia, J. Jasinski, D. Kelly, M. Chhowalla, A. D. Mohite, M. K. Sunkara, G. Gupta, *J. Phys. Chem. C* **2015**, *119*, 22908.
[29] J. Kibsgaard, T. F. Jaramillo, F. Besenbacher, *Nat. Chem.* **2014**, *6*, 248.
[30] H. Wang, Q. Zhang, H. Yao, Z. Liang, H.-W. Lee, P.-C. Hsu, G. Zheng, Y. Cui, *Nano Lett.* **2014**, *14*, 7138.
[31] S. M. Tan, A. Ambrosi, Z. Sofer, Š. Huber, D. Sedmidubský, M. Pumera, *Chem. Eur. J.* **2015**, *21*, 7170.
[32] H. Wang, C. Tsai, D. Kong, K. Chan, F. Abild-Pedersen, J. K. Nørskov, Y. Cui, *Nano Res.* **2015**, *8*, 556.
[33] W. Chen, E. J. G. Santos, W. Zhu, E. Kaxiras, Z. Zhang, *Nano Lett.* **2013**, *13*, 509.
[34] B. Seo, G. Y. Jung, Y. J. Sa, H. Y. Jeong, J. Y. Cheon, J. H. Lee, H. Y. Kim, J. C. Kim, H. S. Shin, S. K. Kwak, S. H. Joo, *ACS Nano* **2015**, *9*, 3728.
[35] Y. Li, H. Wang, L. Xie, Y. Liang, G. Hong, H. Dai, *J. Am. Chem. Soc.* **2011**, *133*, 7296.
[36] C. Tsai, K. Chan, J. K. Nørskov, F. Abild-Pedersen, *Surf. Sci.* **2015**, *640*, 133.
[37] J. Xie, H. Zhang, S. Li, R. Wang, X. Sun, M. Zhou, J. Zhou, X. W. D. Lou, Y. Xie, *Adv. Mater.* **2013**, *25*, 5807.
[38] D. Y. Chung, S.-K. Park, Y.-H. Chung, S.-H. Yu, D.-H. Lim, N. Jung, H. C. Ham, H.-Y. Park, Y. Piao, S. J. Yoo, Y.-E. Sung, *Nanoscale* **2014**, *6*, 2131.
[39] Z. Wu, B. Fang, Z. Wang, C. Wang, Z. Liu, F. Liu, W. Wang, A. Alfantazi, D. Wang, D. P. Wilkinson, *ACS Catal.* **2013**, *3*, 2101.
[40] J. Lin, Z. Peng, G. Wang, D. Zakhidov, E. Larios, M. J. Yacaman, J. M. Tour, *Adv. Energy Mater.* **2014**, *4*, 1301875, DOI:10.1002/aenm.201301875.
[41] Y. Yu, S.-Y. Huang, Y. Li, S. N. Steinmann, W. Yang, L. Cao, *Nano Lett.* **2014**, *14*, 553.
[42] Y. Zhang, Q. Ji, G.-F. Han, J. Ju, J. Shi, D. Ma, J. Sun, Y. Zhang, M. Li, X.-Y. Lang, Y. Zhang, Z. Liu, *ACS Nano* **2014**, *8*, 8617.

[43] A. B. Laursen, S. Kegnæs, S. Dahl, I. Chorkendorff, *Energy Environ. Sci.* **2012**, *5*, 5577.
[44] H. Wang, D. Kong, P. Johanes, J. J. Cha, G. Zheng, K. Yan, N. Liu, Y. Cui, *Nano Lett.* **2013**, *13*, 3426.
[45] D. Merki, S. Fierro, H. Vrubel, X. Hu, *Chem. Sci.* **2011**, *2*, 1262.
[46] H. Vrubel, D. Merki, X. Hu, *Energy Environ. Sci.* **2012**, *5*, 6136.
[47] J. Xie, J. Zhang, S. Li, F. Grote, X. Zhang, H. Zhang, R. Wang, Y. Lei, B. Pan, Y. Xie, *J. Am. Chem. Soc.* **2013**, *135*, 17881.
[48] J. Hong, Z. Hu, M. Probert, K. Li, D. Lv, X. Yang, L. Gu, N. Mao, Q. Feng, L. Xie, J. Zhang, D. Wu, Z. Zhang, C. Jin, W. Ji, X. Zhang, J. Yuan, Z. Zhang, *Nat. Commun.* **2015**, *6*, 6293.
[49] J. Greeley, T. F. Jaramillo, J. Bonde, I. Chorkendorff, J. K. Nørskov, *Nat. Mater.* **2006**, *5*, 909.
[50] M. Kertesz, R. Hoffmann, *J. Am. Chem. Soc.* **1984**, *106*, 3453.
[51] J. Yang, D. Voiry, S. J. Ahn, D. Kang, A. Y. Kim, M. Chhowalla, H. S. Shin, *Angew. Chem. Int. Ed.* **2013**, *52*, 13751.
[52] J. Yuan, J. Wu, W. J. Hardy, P. Loya, M. Lou, Y. Yang, S. Najmaei, M. Jiang, F. Qin, K. Keyshar, H. Ji, W. Gao, J. Bao, J. Kono, D. Natelson, P. M. Ajayan, J. Lou, *Adv. Mater.* **2015**, *27*, 5605.
[53] G. Eda, T. Fujita, H. Yamaguchi, D. Voiry, M. Chen, M. Chhowalla, *ACS Nano* **2012**, *6*, 7311.
[54] S. S. Chou, N. Sai, P. Lu, E. N. Coker, S. Liu, K. Artyushkova, T. S. Luk, B. Kaehr, C. J. Brinker, *Nat. Commun.* **2015**, *6*, 8311.
[55] M. Kan, J. Y. Wang, X. W. Li, S. H. Zhang, Y. W. Li, Y. Kawazoe, Q. Sun, P. Jena, *J. Phys. Chem. C* **2014**, *118*, 1515.
[56] X. Qian, J. Liu, L. Fu, J. Li, *Science* **2014**, *346*, 1344.
[57] M. Calandra, *Phys. Rev. B* **2013**, *88*, 245428.
[58] A. P. Nayak, T. Pandey, D. Voiry, J. Liu, S. T. Moran, A. Sharma, C. Tan, C.-H. Chen, L.-J. Li, M. Chhowalla, J.-F. Lin, A. K. Singh, D. Akinwande, *Nano Lett.* **2015**, *15*, 346.
[59] J. Zhang, M. B. Vukmirovic, Y. Xu, M. Mavrikakis, R. R. Adzic, *Angew. Chem. Int. Ed.* **2005**, *44*, 2132.
[60] W.-F. Chen, K. Sasaki, C. Ma, A. I. Frenkel, N. Marinkovic, J. T. Muckerman, Y. Zhu, R. R. Adzic, *Angew. Chem. Int. Ed.* **2012**, *51*, 6131.
[61] L. Qu, Y. Liu, J.-B. Baek, L. Dai, *ACS Nano* **2010**, *4*, 1321.
[62] R. Silva, D. Voiry, M. Chhowalla, T. Asefa, *J. Am. Chem. Soc.* **2013**, *135*, 7823.
[63] Z. Yang, Z. Yao, G. Li, G. Fang, H. Nie, Z. Liu, X. Zhou, X. Chen, S. Huang, *ACS Nano* **2012**, *6*, 205.
[64] Y. Jiao, Y. Zheng, M. Jaroniec, S. Z. Qiao, *J. Am. Chem. Soc.* **2014**, *136*, 4394.
[65] Y. Zhou, Q. Su, Z. Wang, H. Deng, X. Zu, *Phys. Chem. Chem. Phys.* **2013**, *15*, 18464.
[66] D. B. Putungan, S.-H. Lin, J.-L. Kuo, *Phys. Chem. Chem. Phys.* **2015**, *17*, 21702.
[67] C. Tsai, F. Abild-Pedersen, J. K. Nørskov, *Nano Lett.* **2014**, *14*, 1381.
[68] A. J. Bard, L. R. Faulkner, *Electrochemical Methods: Fundamentals and Applications*, Wiley, New York **2000**.
[69] G. Eda, H. Yamaguchi, D. Voiry, T. Fujita, M. Chen, M. Chhowalla, *Nano Lett.* **2011**, *11*, 5111.
[70] X. Ren, Q. Ma, H. Fan, L. Pang, Y. Zhang, Y. Yao, X. Ren, S. F. Liu, *Chem. Commun.* **2015**, *51*, 15997.
[71] A. Fujishia, K. Honda, *Nature* **1972**, *238*, 37.
[72] M. S. Dresselhaus, I. L. Thomas, *Nature* **2001**, *414*, 332.
[73] Q. Xiang, J. Yu, M. Jaroniec, *J. Am. Chem. Soc.* **2012**, *134*, 6575.
[74] U. Maitra, U. Gupta, M. De, R. Datta, A. Govindaraj, C. N. R. Rao, *Angew. Chem. Int. Ed.* **2013**, *52*, 13057.
[75] Y. Hou, A. B. Laursen, J. Zhang, G. Zhang, Y. Zhu, X. Wang, S. Dahl, I. Chorkendorff, *Angew. Chem. Int. Ed.* **2013**, *52*, 3621.
[76] B. Seger, A. B. Laursen, P. C. K. Vesborg, T. Pedersen, O. Hansen, S. Dahl, I. Chorkendorff, *Angew. Chem. Int. Ed.* **2012**, *51*, 9128.
[77] X. Zong, H. Yan, G. Wu, G. Ma, F. Wen, L. Wang, C. Li, *J. Am. Chem. Soc.* **2008**, *130*, 7176.
[78] W. Zhou, Z. Yin, Y. Du, X. Huang, Z. Zeng, Z. Fan, H. Liu, J. Wang, H. Zhang, *Small* **2013**, *9*, 140.
[79] M.-Q. Yang, C. Han, Y.-J. Xu, *J. Phys. Chem. C* **2015**, *119*, 27234.
[80] F. A. Frame, F. E. Osterloh, *J. Phys. Chem. C* **2010**, *114*, 10628.
[81] J. Chen, X.-J. Wu, L. Yin, B. Li, X. Hong, Z. Fan, B. Chen, C. Xue, H. Zhang, *Angew. Chem.* **2015**, *127*, 1226.
[82] K. Chang, Z. Mei, T. Wang, Q. Kang, S. Ouyang, J. Ye, *ACS Nano* **2014**, *8*, 7078.
[83] F. Meng, J. Li, S. K. Cushing, M. Zhi, N. Wu, *J. Am. Chem. Soc.* **2013**, *135*, 10286.
[84] Y. Sang, Z. Zhao, M. Zhao, P. Hao, Y. Leng, H. Liu, *Adv. Mater.* **2015**, *27*, 363.
[85] T. Jia, A. Kolpin, C. Ma, R. C.-T. Chan, W.-M. Kwok, S. C. E. Tsang, *Chem. Commun.* **2014**, *50*, 1185.
[86] S. Min, G. Lu, *J. Phys. Chem. C* **2012**, *116*, 25415.
[87] M. Liu, F. Li, Z. Sun, L. Ma, L. Xu, Y. Wang, *Chem. Commun.* **2014**, *50*, 11004.
[88] B. Mahler, V. Hoepfner, K. Liao, G. A. Ozin, *J. Am. Chem. Soc.* **2014**, *136*, 14121.
[89] M. Bernardi, M. Palummo, J. C. Grossman, *Nano Lett.* **2013**, *13*, 3664.
[90] X. Zong, J. Han, G. Ma, H. Yan, G. Wu, C. Li, *J. Phys. Chem. C* **2011**, *115*, 12202.
[91] H. L. Zhuang, R. G. Hennig, *J. Phys. Chem. C* **2013**, *117*, 20440.
[92] J. Kang, S. Tongay, J. Zhou, J. Li, J. Wu, *Appl. Phys. Lett.* **2013**, *102*, 012111.
[93] Y. Guo, D. Sun, B. Ouyang, A. Raja, J. Song, T. F. Heinz, L. E. Brus, *Nano Lett.* **2015**, *15*, 5081.
[94] J. Heising, M. G. Kanatzidis, *J. Am. Chem. Soc.* **1999**, *121*, 11720.
[95] E. Parzinger, B. Miller, B. Blaschke, J. A. Garrido, J. W. Ager, A. Holleitner, U. Wurstbauer, *ACS Nano* **2015**, *9*, 11302.